Available online at www.sciencedirect.com
SCIENCE DIRECT®
Carbohydrate Research 340 (2005) 2510–2519
Carbohydrate RESEARCH

Characterisation of Ca– and Al–pectate gels by thermal analysis and FT-IR spectroscopy

Tanja Mimmo,* Claudio Marzadori, Daniela Montecchio and Carlo Gessa

Department of Agroenvironmental Sciences and Technologies—Alma Mater Studiorum, University of Bologna, Viale Fanin 40, 40127 Bologna, Italy

Received 16 June 2005; received in revised form 24 August 2005; accepted 26 August 2005
Available online 5 October 2005

Abstract—Thermal analysis (TG–DTA) and FT-IR spectroscopy have been performed on calcium–pectate membranes to investigate their structure and the consequent variation caused by aluminium sorption. Calcium–polygalacturonate (Ca–PG) membranes, model systems of the soil–root interface, were exposed to aluminium solutions at different concentrations (25–800 μM). Three different pHs (3.50, 4.00 and 4.50) were chosen to study the influence of different aluminium species, such as $[Al(H_2O)_6]^{3+}$, $[Al(OH)(H_2O)_5]^{2+}$ and $[Al(OH)_2(H_2O)_4]^{+}$, on the structure of the Ca–PG membrane. The DTA profiles and FT-IR spectra showed how aluminium sorption induces structural modifications leading to a reorganisation of the chain aggregates and a weakening of the structure. Higher pH, that is, 4.00 and 4.50, and thus hydrolytic aluminium species and related higher calcium content maintain a more regular structure than at pH 3.50. At pH 3.50, both the effect of $[Al(H_2O)_6]^{3+}$ and a major calcium release had a greater impact and thus induced a greater weakening of the structure.

Keywords: Polygalacturonic acid; Calcium; Aluminium; FT-IR spectroscopy; TG–DTA

1. Introduction

Pectins are common plant polysaccharides that have various applications in both the pharmaceutical and food industry.[1] Besides these technological applications, they play an important role in plant physiology. One of the major properties of pectins is their ability to form gels in the presence of calcium (Ca^{2+}) ions, promoting the formation of secondary structure. Two or more saccharidic chains are involved in a cooperative binding mechanism leading to the well known 'egg-box' model.[2] This three-dimensional network consists of double helical junction zones with the ability to hold water and provide mechanical support. The Ca^{2+} ions are complexed by oxygen atoms (O_5, O_6 and O_2) from one chain with oxygen atoms (O_6 and O_2) from an antiparallel adjacent chain.[3,4] Water molecules complete an eight or ninefold calcium coordination shell. In this way, calcium acts as an ion bridge between two chains.[5]

Ca–pectates are largely found at the soil–root interface and are the major high molecular weight compounds exuded by roots. They constitute the so-called mucilage, which plays a key role in the cation exchange capacity of root cell walls. These properties explain their ability to form complexes with heavy metals, for example Pb^{2+} and Cd^{2+}, as well as micronutrients. This results in a diffusive exchange[6,7] due to their acidic properties. In fact, the electronegative carboxylate groups present on the Ca–pectate matrix do not permit free diffusion through the matrix but retain ions and are thus exchangeable. In addition, they may help to desorb anions usually poorly soluble in soil such as phosphate from soil mineral aggregates.[8] Other benefits have been ascribed to the mucilage, including establishing continuity between the roots and solid soil particles. The mucilage improves the water transfer towards the roots.[9] The root mucilage is made mainly out of calcium–pectates, namely fibrils of calcium–polygalacturonate (Ca–PG).[10–12] A number of

* Corresponding author. Tel.: +39 051 2096207; fax: +39 051 2096203; e-mail: tmimmo@agrsci.unibo.it

0008-6215/$ - see front matter © 2005 Elsevier Ltd. All rights reserved.
doi:10.1016/j.carres.2005.08.011

papers have reported studies of the adsorption mechanisms of metals using a Ca–PG membrane as a system model.[13–15] In these investigations, it was shown as to how the characteristic fibrillar structure is modified by the interaction of the metals with the membrane. For example, it was demonstrated that aluminium hindered water transfer.[16] Aluminium, a well known toxic element for plants, is mainly bound to the negative charged binding sites of pectins found in both the apoplast and the soil–root interface. Aluminium toxicity differs with its interaction, especially between $[Al(H_2O)_6]^{3+}$ and mononuclear hydroxyl-Al. Generally, $[Al(H_2O)_6]^{3+}$ is more phytotoxic to plants than $[Al(OH)(H_2O)_5]^{2+}$ and $[Al(OH)_2(H_2O)_4]^{+}$ but some authors[17,18] reported that dicotyledonous plants may be more sensitive to hydrolytic species than $[Al(H_2O)_6]^{3+}$. Structural investigations of the interaction of aluminium with the pectic compounds would help to better understand metal toxicity. To date, there have been very few studies on the interaction of trivalent cations[19–21] with pectates, while the interaction with bivalent cations like Ca^{2+}, Ni^{2+}, Zn^{2+}, Cd^{2+} and Pb^{2+} has been extensively studied, for example, by FT-IR spectroscopy.[22–25] This technique has proven to be a very powerful and sensitive approach for investigating the structure, physical properties and interactions of carbohydrates, including pectins.[26,27] Various cations might induce different chain associations and thus different configurations and different ion sizes and charge densities lead to shifts of the characteristic absorption bands of carbohydrates both in the carboxylate region (1600–1400 cm^{-1}) and in C–O ring vibrations in the 1200–900 cm^{-1} region. In addition, thermal analysis has been used to investigate the degradation of pure cellulose and its interaction with organometallic additives.[28,29] The coupling of FT-IR spectroscopy with thermal analysis could therefore improve the understanding of structural modifications as already shown in a study on the functional evolution of cellulose.[30] In addition, the oxidative reactivity of pectins and related carbohydrates by these methods has been recently studied.[31]

In the present study, both techniques, FT-IR spectroscopy and thermal analysis, were used to investigate the influence of aluminium on the Ca–pectate structure. A model system made out of Ca–PG was used to simulate the soil–root interface. The speciation of the metal was also taken into account by conducting the sorption at different pH levels. The aim was to characterise the structural modifications induced by both effects.

2. Results and discussion

2.1. Compositional analysis

Table 1 shows the calculated molar fractions of the Ca–PG and Ca–Al–PG networks. As can be seen, the molar fractions increase with aluminium concentration within each pH level but decrease with increasing pH. These results are also supported by the regression analysis of the calcium release and aluminium adsorbed as a function of the aluminium concentration used to form the Ca–Al–PG networks (Fig. 1). At pH 3.50 and 4.00 (25–800 μM, Fig. 1a and b), the results show an exponential fit for both calcium release and aluminium sorption and the correlation coefficients (r) indicate a relatively strong relationship between the variables.

Table 1. Aluminium molar fractions (Al/(Al + Ca)) of the Ca–PG and Ca–Al–PG networks (nd = not determined)

Network	pH 3.50	pH 4.00	pH 4.50
Ca–PG	0.00	0.00	0.00
Ca–Al25–PG	0.15	0.05	0.05
Ca–Al50–PG	0.29	0.12	0.13
Ca–Al100–PG	0.39	0.25	0.26
Ca–Al200–PG	0.53	0.42	nd
Ca–Al400–PG	0.81	0.71	nd
Ca–Al800–PG	0.85	0.81	nd

On the contrary, at pH 4.50 (25–100 μM, Fig. 1c) the results show a linear fitting for both calcium release and aluminium sorption. This is due to the lower range of aluminium concentrations, that is, 25–100 μM, which were chosen to avoid the presence of polymeric species as can be seen in Figure 2 where their distribution is plotted as a function of pH. At concentrations as high as 200–800 μM, there would be 74% of $Al_{13}O_4(OH)_{24}^{7+}$ present in the solution. At lower pH, statistical analysis confirms a relatively strong relationship between the variables.

Regression analysis was also carried out for low aluminium concentrations, that is, 25–100 μM to compare better the different chemical compositions at the three pH levels (insets in Fig. 1). At pH 3.50, the best fit resulted in a square root x-model to describe the relationship between calcium release and aluminium concentration, whereas the relationship between aluminium sorption and aluminium concentration was again described by an exponential model. At higher pH, both aluminium sorption and calcium release are described by a linear model. In particular, there are no significant differences between calcium release and aluminium sorption (insets in Fig. 1b and c) suggesting an equimolar ratio of the two variables.

These varying behaviours could be the result of the different speciations of aluminium (Fig. 2). $[Al(H_2O)_6]^{3+}$ is the predominant species (97%) at pH 3.50, whereas at pH 4.00 $[Al(H_2O)_6]^{3+}$ is reduced to 90% and at pH 4.50 to 71%. Even the low percentages of hydrolytic species (10% at pH 4.00 and 29% at pH 4.50) present in solution seem thus to considerably influence the chemical composition of the Ca–Al–PG networks. The trends observed at the three pH levels could be explained by

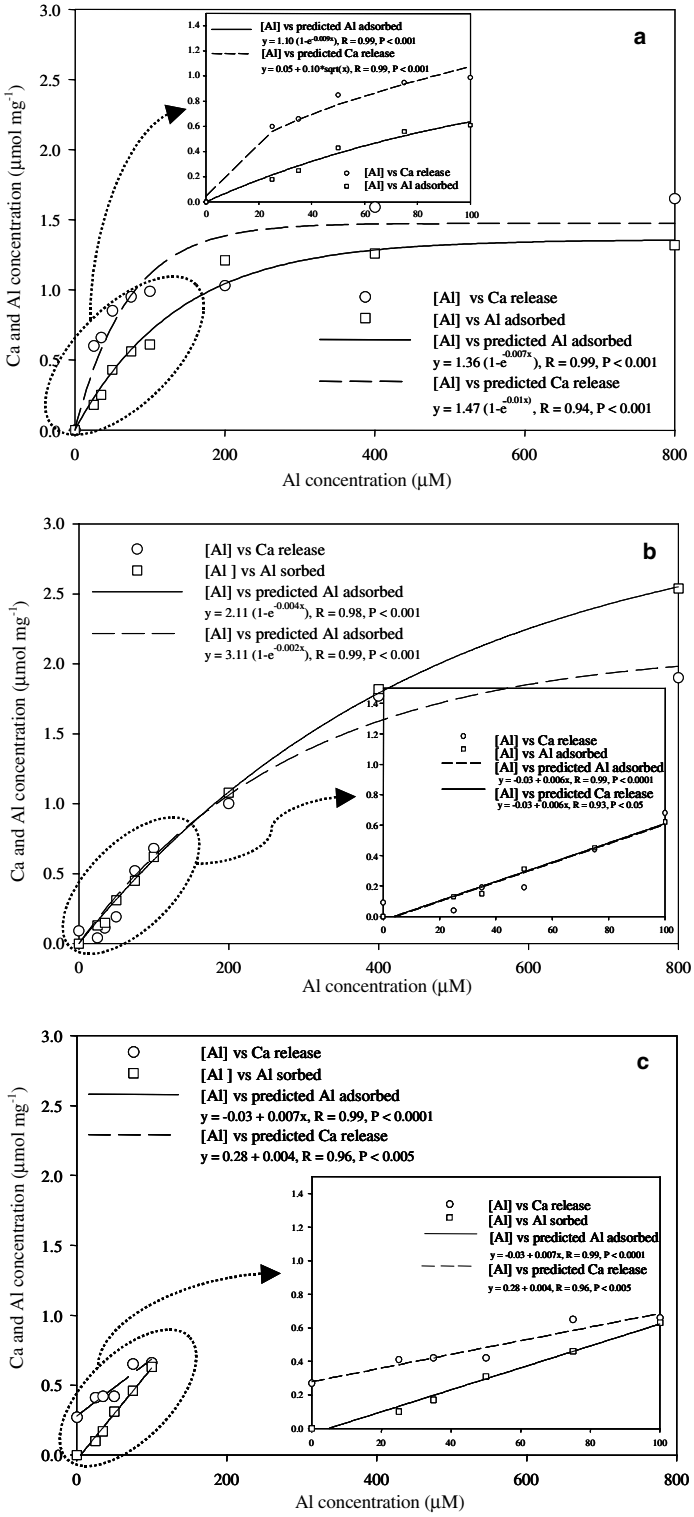

Figure 1. Correlation plots of calcium release and content versus aluminium concentration (0–800 µM) used to form the Ca–Al–PG networks: (a) pH 3.50, (b) pH 4.00 and (c) 4.50; error bars are not shown. In each plot, insets show the correlations obtained in a lower concentration range (0–100 µM).

an increasing aluminium competition for the reticulation sites as the pH decreases (pH 4.50 > 4.00 > 3.50). These different chemical compositions could lead to variations and reorganisation of the structure of the networks, which was further investigated by thermal analysis and FT-IR spectroscopy.

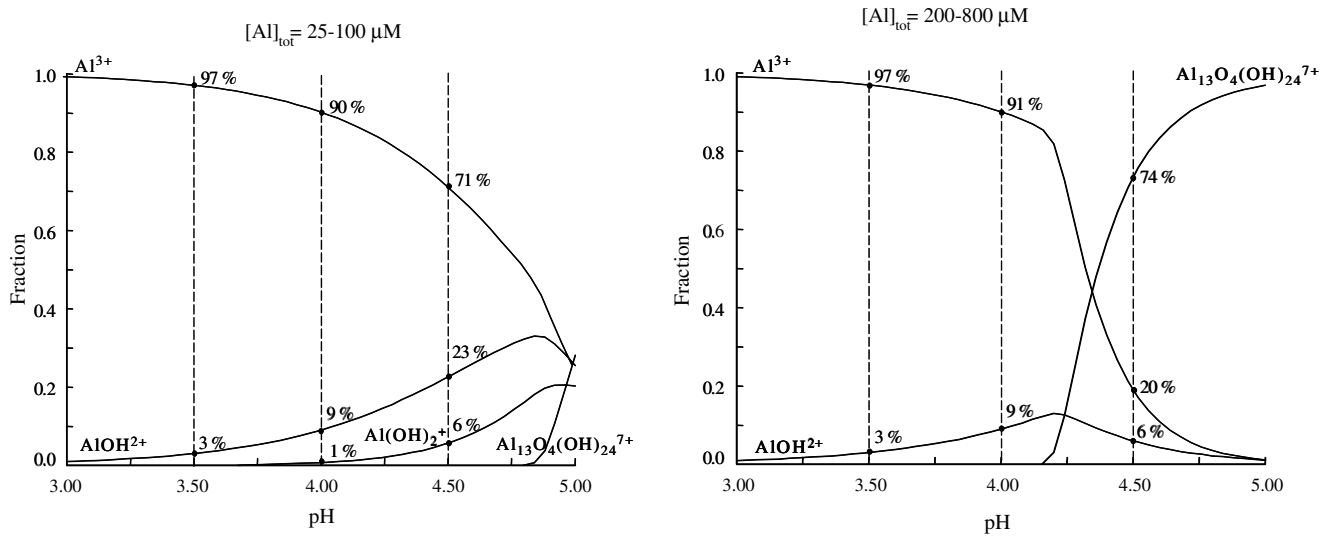

Figure 2. Distribution of aluminium species (aluminium fraction vs pH): on the left concentration range from 25 to 100 µM, on the left concentration range from 200 to 800 µM.

2.2. Thermal analysis

Figure 3 shows the DTA curves of the thermal decomposition in air of the Ca–PG and Ca–Al–PG networks at the three pH levels studied. All the freeze-dried samples revealed a first endothermic peak due to dehydration (average mass loss of 19%) that are not shown in the profiles. The other peaks detected are all exothermic and their corresponding temperatures (T_{max}) and weight losses (TG) are reported in Table 2.

The DTA curves of the Ca–PG networks did not vary as a function of pH. The profiles show very well defined and well separated peaks, the first one around 300 °C ($\Delta m = 39\%$) and a second, broader one around 450 °C ($\Delta m = 5.5\%$). These could be considered as the result of a partial decarboxylation reaction of protonated carboxylates, oxidation reactions of small fragments of the polygalacturonate ring and/or the opening of the pyranoid rings present on the polygalacturonate chains, respectively.[32] A more intense exothermic decomposition reaction took place at 580 °C with a mass loss of around 17%. The high oxidation temperature is probably caused by the decomposition of the part of the polygalacturonate chain that is coordinated to the metal, that is, calcium ions complexed by carboxylate and other functional groups (OH and O) of the pyranoid ring.

For the DTA curves obtained at pH 3.50, aluminium molar fractions as low as 0.15 have a great effect on the structure. Indeed, the peak at 580 °C in Ca–PG is split into two exothermic peaks in Ca–Al25–PG: one at 448 °C ($\Delta m = 11.8\%$) and the other one at 606 °C ($\Delta m = 4.2\%$). Calcium and aluminium ions are probably coordinated in a different way by the polygalacturonate chains, which cause different thermal behaviour and thus two exothermic peaks. As aluminium causes a decrease in the temperature of the main exothermic peak (around 450 °C in Ca–Al25–PG and Ca–Al100–PG), it is most likely that it forms less stable complexes with the network. All these exothermic peaks are well defined and well separated only to an aluminium molar fraction of 0.39 (Table 1), which seems to be the breaking point. At or below a molar fraction of 0.39, the calcium concentration seems to be high enough to coordinate the polygalacturonate chains in an ordered way leading to a regular well organised structure, while at aluminium molar fractions of 0.53, 0.81 and 0.85, aluminium becomes the predominant ion, which appears to destroy the network. Indeed, at these higher aluminium concentrations the thermal profiles get more and more disordered, that is, no well defined decomposition reactions take place suggesting one continuous reaction.

At pH 4.00, the decomposition profiles had the same trend as pH 3.50 (Fig. 3). The first exothermic peak at 305 °C corresponds most probably to the partial decarboxylation of the protonated carboxylic groups and oxidation reactions of small fragments of the polygalacturonate chains. The T_{max} of this peak does not vary with increasing aluminium concentration, although its intensity increases considerably. In Ca–PG it corresponds to a mass loss of 39% whereas in Ca–Al100–PG, the peak at 302 °C almost doubles its intensity having a mass loss of 51%.

The opening of the pyranoid rings leads to the second exothermic peak at 448 °C that does not change its position. Similar to the first one, the intensity of this peak increases with increasing aluminium concentration becoming a very sharp peak in Ca–Al100–PG. As previously observed at pH 3.50, only aluminium

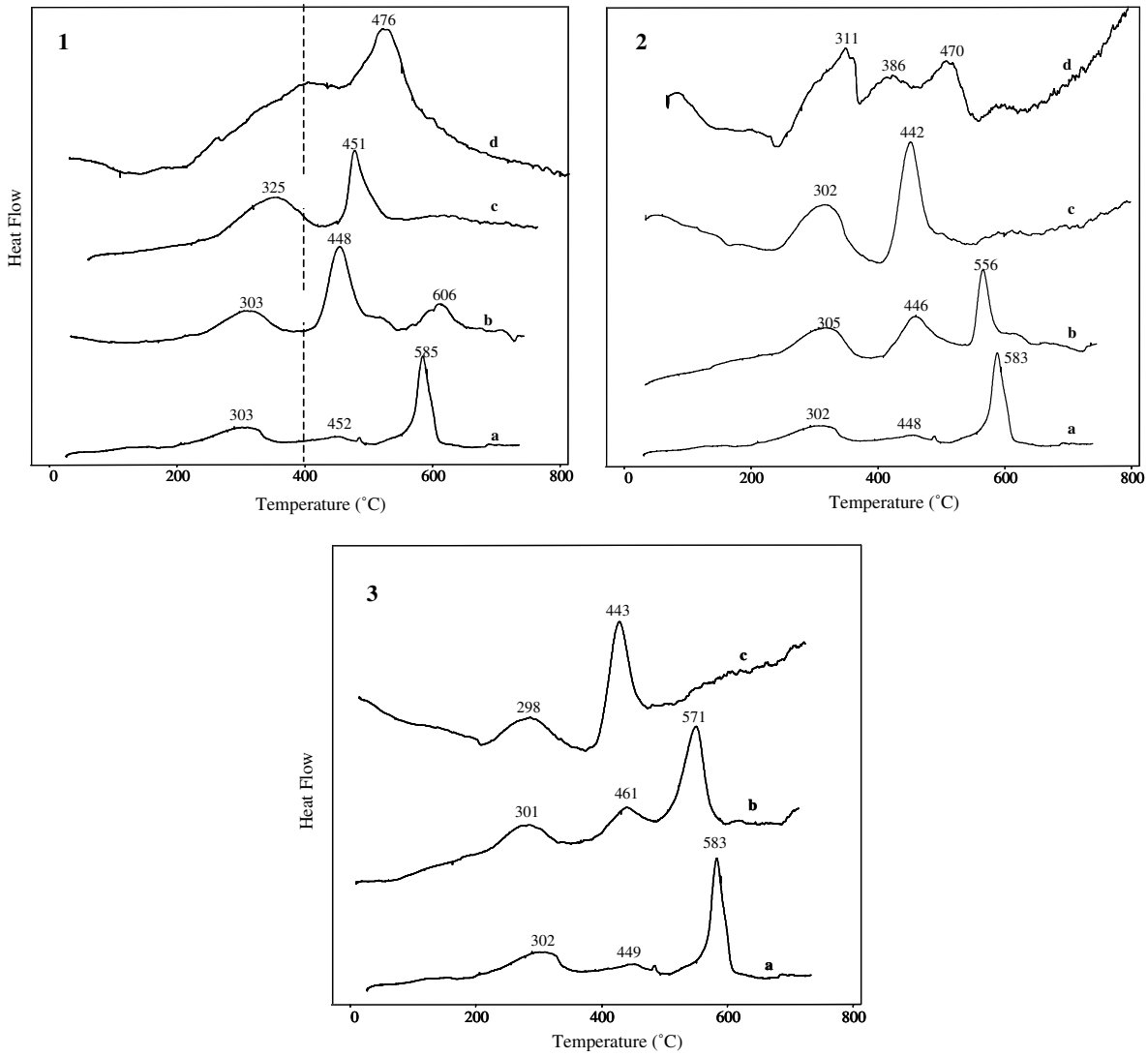

Figure 3. DTA curves under air flow of (a) Ca–PG, (b) Ca–Al25–PG, (c) Ca–Al100–PG and (d) Ca–Al800–PG at (1) pH 3.50, (2) pH 4.00 and (3) pH 4.50.

Table 2. TG–DTA data obtained under air atmosphere of the Ca–PG and Ca–Al–PG at the three pHs studied

Sample	1° exo		2° exo		3° exo	
	T_{max} (°C)	Mass loss (%)	T_{max} (°C)	Mass loss (%)	T_{max} (°C)	Mass loss (%)
pH 3.50						
Ca–PG	302 ± 1	39.2 ± 0.4	448 ± 2	5.5 ± 0.5	583 ± 2	17.2 ± 0.6
Ca–Al25–PG	303 ± 2	43.2 ± 0.5	448 ± 1	11.8 ± 0.3	606 ± 3	4.2 ± 0.4
Ca–Al100–PG	325 ± 1	57.9 ± 0.3	451 ± 3	16.8 ± 0.8	—	—
Ca–Al800–PG	365 ± 3	58.1 ± 0.1	471 ± 2	23.5 ± 0.7	—	—
pH 4.00						
Ca–PG	302 ± 2	39.2 ± 0.3	448 ± 2	5.5 ± 0.2	583 ± 1	17.2 ± 0.4
Ca–Al25–PG	305 ± 3	38.1 ± 0.5	446 ± 1	11.8 ± 0.6	556 ± 3	10.2 ± 0.2
Ca–Al100–PG	302 ± 1	51.0 ± 0.8	442 ± 3	24.2 ± 0.5	—	—
Ca–Al800–PG	311 ± 2	41.0 ± 0.6	386 ± 1	—	470 ± 3	28.0 ± 0.3
pH 4.50						
Ca–PG	302 ± 1	39.2 ± 0.5	448 ± 2	5.5 ± 0.3	583 ± 2	17.2 ± 0.3
Ca–Al25–PG	301 ± 3	36.7 ± 0.3	461 ± 1	10.4 ± 0.2	571 ± 1	15.5 ± 0.5
Ca–Al100–PG	298 ± 4	33.8 ± 0.2	443 ± 1	15.1 ± 0.2	—	—

Only exothermic reactions are reported ($n = 3$, mean ± standard deviation).

molar fractions up to 0.26 keep a somewhat ordered structure; higher values lead to poorly defined thermal profiles. However, this behaviour is more noticeable at lower pH most likely because of lower calcium content and a higher proton effect. At pH 4.50, the decomposition profiles are almost the same as the one at pH 4.00.

These results suggest that aluminium sorption alters the structure more at lower pH. Indeed, at pH 3.50 the main species present in solution is $[Al(H_2O)_6]^{3+}$ (97%) leading to a drastic calcium release, especially at high aluminium molar fractions. For instance, the weight loss of the first exothermic peaks decreases noticeably (pH 3.50 > pH 4.00 > pH 4.50, Table 2) as more carboxylic groups are protonated at pH 3.50.

At higher pHs as at 4.00 and 4.50, both the larger calcium content and the presence of hydrolytic species ($[Al(OH)(H_2O)_5]^{2+}$ and $[Al(OH)_2(H_2O)_4]^{+}$) could prevent the collapse of the structure. First, higher calcium content leads to a more ordered structure. Second, hydrolytic species having a lower electric charge present a lower affinity for the coordination sites of the polygalacturonate chains and thus these species have a minor exchange activity. In addition, it cannot be excluded that within the networks polymeric forms of aluminium could be formed thus influencing considerably the conformation of the polygalacturonate chains.

The Ca–PG and Ca–Al–PG networks obtained at pH 3.50 were also analysed under a dynamic nitrogen atmosphere to further investigate structural modifications induced by the monomeric aluminium species $[Al(H_2O)_6]^{3+}$. All the first derivatives of the thermogravimetric curves (DTG) show two very distinct peaks (Fig. 4). The Ca–PG networks reveal a first peak at 80 °C ($\Delta m = 19\%$) and a sharper one at 265 °C ($\Delta m = 29\%$). The first one is the result of the loss of water molecules present in the coordination sphere of the Ca–PG complex, whereas the second peak could be due to the breakdown of the polymer. The presence of aluminium shifts the first peak towards higher temperatures with decreasing weight losses: aluminium could retain less water but it is stronger than calcium in its coordination sphere, except for Ca–Al800–PG (aluminium molar fraction of 0.85). One interpretation could be that at high aluminium concentrations, the disorder of the structure causes an increase in bound water but with only minor hydration energy.

The second peak at 260 °C is shifted towards lower temperatures with increasing weight loss (from 29% to 46%). This trend is almost the opposite at the maximum molar fraction of aluminium, that is, 0.85, where the first peak is again found at 82 °C with a mass loss of 27%, whereas the second follows the previous trend and is shifted towards a lower temperature (229 °C). These profiles point out a strong impact of $[Al(H_2O)_6]^{3+}$. Thermal decomposition takes place at lower temperatures if aluminium becomes the predominant reticulating ion and the calcium content is negligible.

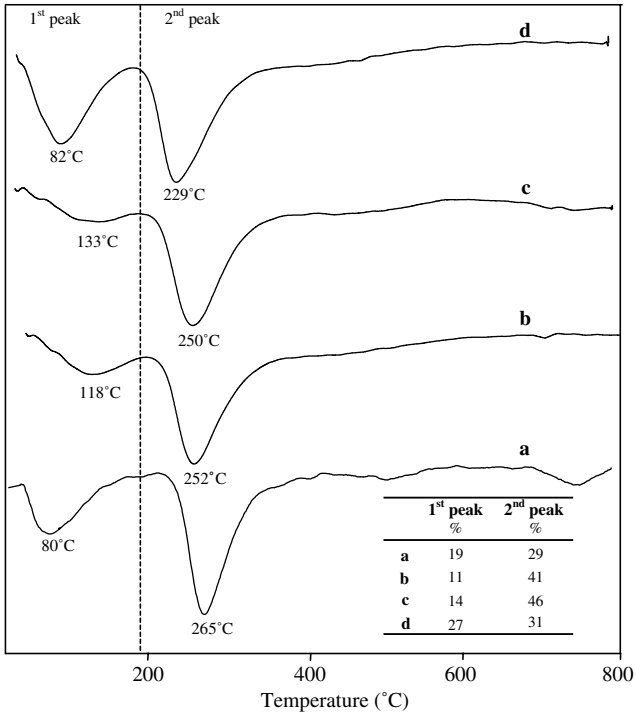

	1st peak %	2nd peak %
a	19	29
b	11	41
c	14	46
d	27	31

Figure 4. First derivative of the thermogravimetric curves (DTG) under nitrogen flow of (a) Ca–PG, (b) Ca–Al25–PG, (c) Ca–Al100–PG and (d) Ca–Al800–PG obtained at pH 3.50. The table shows the weight losses of the two detected peaks of each profile.

2.3. FT-IR spectroscopy

Figure 5 shows the FT-IR spectra of the Ca–PG and Ca–Al–PG networks at different concentrations and pH levels. At all pH levels, aluminium sorption induces shifts of the characteristic bands of carbohydrates in both the carboxylate region (1700–1400 cm^{-1}) and the anomeric region (1200–900 cm^{-1}). The spectral changes at pH 3.50 have already been extensively discussed.[33] In accordance with the egg-box model hypothesis,[34,35] a multidentate coordination of both calcium and aluminium with the polygalacturonate chains was proposed, which involves the carboxylate group, the ring oxygen, the glycosidic oxygen, a hydroxyl group from the next galacturonic residue and two water molecules.

Tables 3 and 4 show the carboxylate stretching frequencies of the networks obtained at the three pH levels and the difference (Δ) between the asymmetric, ν_{as} (COO^-), and the symmetric, ν_s (COO^-), stretching frequencies. At pH 3.50 and 4.00, the major effect of aluminium sorption is the shift of the ν_{as} (COO^-) leading to an increase of the Δ from 184 cm^{-1} in Ca–PG to 201 cm^{-1} in Ca–Al800–PG at pH 3.50 and from 184 cm^{-1} to 200 cm^{-1} at pH 4.00. In addition, the ν_{as}

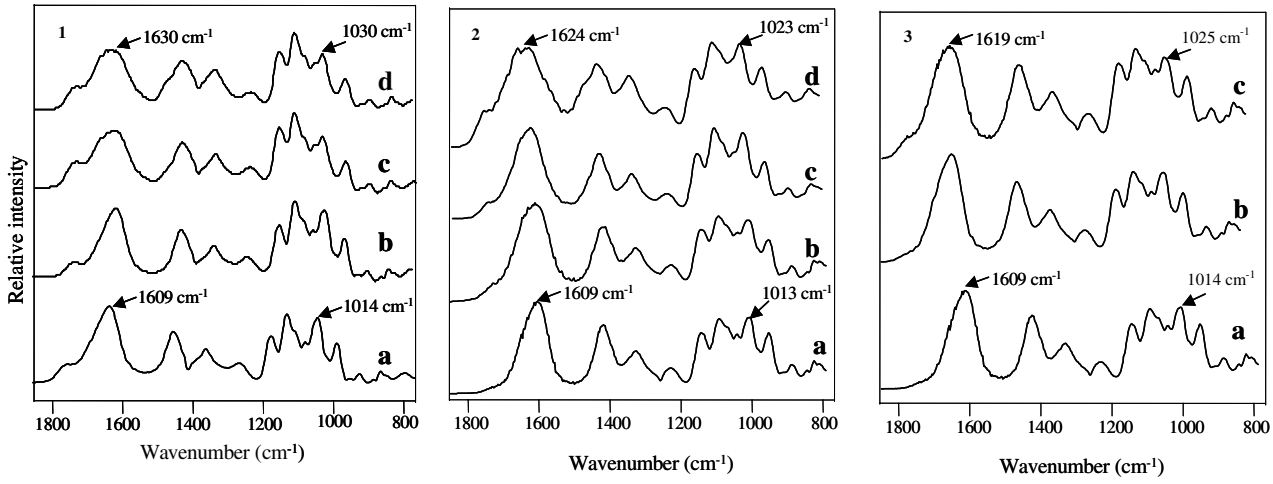

Figure 5. FT-IR spectra of (a) Ca–PG, (b) Ca–Al25–PG, (c) Ca–Al100–PG and (d) Ca–Al800–PG at (1) pH 3.50, (2) pH 4.00 and (3) pH 4.50.

Table 3. Carboxylate stretching frequencies (cm^{-1}) and difference between ν_{as} (COO^-) and ν_s (COO^-) of Ca–PG and Ca–Al–PG networks (as is and heated up to 400 °C) at pH 3.50

Network	As is			After 400 °C		
	ν_{as} (COO)	ν_s (COO^-)	$\Delta = \nu_{as} - \nu_s$	ν_{as} (COO^-)	ν_s (COO^-)	$\Delta = \nu_{as} - \nu_s$
Ca–PG	1609	1425	184	1570	1416	154
Ca–Al25–PG	1611	1426	185	1566	1407	159
Ca–Al50–PG	1617	1427	190	1570	1415	155
Ca–Al100–PG	1618	1428	190	1575	1417	158
Ca–Al200–PG	1628	1430	198	1574	1417	157
Ca–Al400–PG	1626	1430	196	1585	1410	175
Ca–Al800–PG	1630	1429	201	1585	1410	175

Table 4. Carboxylate stretching frequencies (cm^{-1}) and difference between ν_{as} (COO^-) and ν_s (COO^-) of Ca–PG and Ca–Al–PG networks at pH 4.00 and 4.50

Network	pH 4.00			pH 4.50		
	ν_{as} (COO^-)	ν_s (COO^-)	$\Delta = \nu_{as} - \nu_s$	ν_{as} (COO^-)	ν_s (COO^-)	$\Delta = \nu_{as} - \nu_s$
Ca–PG	1609	1425	184	1609	1425	184
Ca–Al25–PG	1616	1423	193	1608	1426	182
Ca–Al50–PG	1616	1420	196	1609	1419	190
Ca–Al100–PG	1618	1421	197	1619	1425	194
Ca–Al200–PG	1617	1425	192	nd	nd	nd
Ca–Al400–PG	1617	1421	196	nd	nd	nd
Ca–Al800–PG	1624	1424	200	nd	nd	nd

(COO^-) band broadens with increasing aluminium concentration with the appearance of a shoulder at 1700 cm^{-1} most likely as a result of protonation of the carboxylate groups. This would indicate that more protonated groups lead to less reticulation sites and a greater presence of water. However, this shoulder is more marked at pH 3.50 indicating that at lower pH levels the proton effect is much stronger as was previously observed in the DTG curves.

Further band shifts can be observed in the region between 1200 and 900 cm^{-1}. In this region, bands arise from coupled C–C and C–O vibration modes of the polygalacturonate rings, their hydroxyl groups and glycosidic linkage. Aluminium sorption causes a shift in the stretching frequency of the functional groups (C–O, C–C) present on the pyranoid units of the polygalacturonate chain shifts. These changes are from 1014 cm^{-1} in Ca–PG to 1030 cm^{-1} in Ca–Al800–PG at pH 3.50 and from 1013 cm^{-1} to 1023 cm^{-1} at pH 4.00 (Table 5 and Fig. 3). Additionally, the relative intensity of the 'anomeric' bands increases with respect to the ν_{as} (COO^-) and ν_s (COO^-) as the aluminium concentration increases. In Ca–Al800–PG, the bands in both regions reach almost the same relative intensities.

Table 5. Stretching frequencies (cm^{-1}) of the functional groups [ν (C–O, C–C)] present in the pyranoid ring of the polygalacturonate chain; nd = not determined, PG = polygalacturonate

Network	pH 3.50	pH 4.00	pH 4.50
Ca–PG	1014	1014	1014
Ca-A25–PG	1018	1019	1016
Ca–Al50–PG	1027	1021	1013
Ca–Al100–PG	1026	1025	1025
Ca–Al200–PG	1032	1022	nd
Ca–Al400–PG	1029	1023	nd
Ca–Al800–PG	1030	1023	nd

The same trend can be noticed at pH 4.50 even though only low aluminium concentrations were used. The asymmetric carboxylate stretching frequencies shift from 1609 to 1619 cm^{-1}, leading to an increase of the Δ from 184 cm^{-1} in Ca–PG to 194 cm^{-1} in Ca–Al100–PG. Similar values have been found in Ca–Al100–PG at lower pH (190 cm^{-1} at pH 3.50 and 197 cm^{-1} at pH 4.00), indicating that aluminium sorption changes the coordination of the carboxylate groups independent of pH. However, comparing the bands around 1015 cm^{-1} the highest shift of the stretching frequencies of the C–O and C–C groups of the pyranoid ring takes place at pH 3.50, that is, from 1014 to 1030 cm^{-1} (Table 5). This indicates that $[Al(H_2O)_6]^{3+}$ interacts more with the anomeric region than with the carboxylic groups. If $[Al(H_2O)_6]^{3+}$ prevails over the hydrolytic species $[Al(OH)(H_2O)_5]^{2+}$ and $[Al(OH)_2(H_2O)_4]^{+}$, the structure of the polygalacturonate chains is more distorted. Even if both the aluminium and calcium ions seem to form multidentate complexes with the polygalacturonate chains, the trivalent cation causes a rearrangement of the structure of the network. This effect seems more enhanced at pH 3.50 than at 4.00 and 4.50. The FT-IR results suggest that $[Al(H_2O)_6]^{3+}$ leads to a weaker structure even at low aluminium concentrations, whereas hydrolytic species seem to have a minor impact on the structure. These results are also in agreement with the thermal analysis discussed before. Both speciation and different chemical composition between the pH levels lead to different interactions and conformations of the calcium–aluminium–polygalacturonate complexes.

The spectra obtained at the three pH levels were all obtained on freeze-dried samples and reported as 'as is' samples. At pH 3.50, the Ca–PG and Ca–Al–PG networks were heated isothermally to 400 °C and their degradation residues were consequently analysed by FT-IR spectroscopy to further investigate the thermal reaction taking place up to 400 °C (dotted line in Fig. 3-1). As the decomposition took place in an oxidising atmosphere such as air, the spectra of the residue after heating at 400 °C lost their typical shape. The characteristic absorption bands in the anomeric region disappeared completely and the only bands detected were those of the carboxylic acid groups. Table 3 shows the asymmetric, ν_{as} (COO^-), and the symmetric stretching frequencies, ν_s (COO^-) and their differences (Δ). The Δ increases with increasing aluminium concentration for the 'as is' samples as for the decomposition residues (Table 3), which indicates a change of the coordination of the carboxylate groups. The presence of the ν_{as} and ν_s bands supports the idea that the residue remaining after 400 °C is that part of the polymer coordinated to the metal ion, that is, two DTA peaks in Ca–PG and two DTA peaks in Ca–Al–PG (Fig. 3). In addition, the increasing Δ, from 154 to 159 cm^{-1}, with increasing aluminium concentration supports the idea that aluminium induces changes in the coordination of the polygalacturonic chains. This is also visible in the DTA profiles (Fig. 3) where the peak around 580 °C in Ca–PG is split into two peaks, one at 448°C and one at 606 °C in Ca–Al25–PG. These FT-IR results also support that an aluminium molar fraction of 0.39 is the breaking point of the structure: the Δ passes from 158 cm^{-1} in Ca–Al25–PG to 175 cm^{-1} in Ca–Al800–PG.

3. Conclusions

The results obtained by thermal analysis and FT-IR spectroscopy indicate that $[Al(H_2O)_6]^{3+}$ interacts with the polygalacturonate chains in a different way than the hydrolytic $[Al(OH)(H_2O)_5]^{2+}$ and $[Al(OH)_2(H_2O)_4]^{+}$ species. It is most likely that $[Al(H_2O)_6]^{3+}$ interacts in a stronger way with the anomeric part of the polygalacturonate chains than with the carboxylic groups. This is especially apparent when observing the thermal degradation profiles at the three pH levels. FT-IR spectra confirm that at all the pH levels studied, aluminium interacts with the carboxylate groups as well as with the functional groups of the pyranoid ring forming a multidentate complex. The shape of the bands, their broadening and decrease of intensity indicate that aluminium has similar but weaker interactions. The regular egg-box structure of the Ca–PG fibrils evolves into disordered chain associations.

There were considerable differences between the pH levels of the different Al species as the different size and charge density influence the configuration of the polygalacturonate chains. The results would suggest that $[Al(H_2O)_6]^{3+}$ and thus pH 3.50 lead to a greater collapse of the Ca–PG fibrils than the hydrolytic species at pH 4.00 and 4.50. This conclusion would also be in agreement with the chemical composition: a majority of calcium content at higher pH levels could preserve a more regular structure. In addition, as the membranes were also used as a model system of the soil–root interface, these modifications would indicate that $[Al(H_2O)_6]^{3+}$ could inhibit the transport of nutrients and water across the soil–root interface thus influencing considerably plant growth. On the other hand, previous

studies[36] showed that the phosphate flux through a Ca–Al–PG membrane was more hindered at higher pHs than at lower ones. This would suggest that hydrolytic species as $[Al(OH)(H_2O)_5]^{2+}$ and $[Al(OH)_2(H_2O)_4]^{+}$ seem less destructive from the structural point of view, but behave exactly the opposite from a functional point of view. Even if the Ca–Al–PG networks have a less disordered structure at pH 4.00 and 4.50, they would reduce the diffusion of nutrients like phosphate by reduction of the dimension of the pores of the fibrillar network.

4. Experimental

4.1. Samples

Custom-made cells made out of Plexiglas were used to form the Ca–PG and Ca–Al–PG networks. A steel net positioned in the middle of the cell acted as a support of the networks. A gelatinous membrane, the Ca–PG network, was formed on the net with a 0.15 solution of polygalacturonic acid (PGA, Sigma), at pH 4.50, in the presence of Ca^{+2}. The networks obtained were approximately 2–3 mm thick. Once the Ca–PG networks were formed, the cells were filled with a solution of $Al(NO_3)_3$ 9 H_2O (Riedel-de Haën GmbH) at pH 3.50, 4.00 and 4.50 at different concentrations of 0, 25, 35, 50, 75, 100, 200, 400 and 800 μM to obtain Ca–PG, Ca–Al25PG, Ca–Al35–PG, Ca–Al50–PG, Ca–Al75–PG, Ca–Al100–PG, Ca–Al200–PG, Ca–Al400–PG and Ca–Al800PG networks (repeated three times). At pH 4.50, the 200, 400 and 800 μM solutions were not used in order to avoid the formation of polymeric forms of Al. Al speciation was calculated using Species software (©Academic software and K.J. Powell, Vers. 5.14, 1999). Al sorption was conducted for 24 h under constant stirring, and calculated by difference between Al initially present in the solutions and the residual Al present at the end of the sorption procedure. Al concentration was then determined colorimetrically.[37] Statistical analysis was carried out using Statgraphic Plus5 software (Manugistics, Inc., Rockville, MD, USA).

4.2. Thermal analysis

Thermogravimetric (TG) and differential thermal analysis (DTA) were carried out simultaneously using a TG–DTA92 instrument (SETARAM, France). About 5 mg of freeze-dried networks (Ca–PG and Ca–Al–PG obtained at pH 3.50, 4.00 and 4.50) was weighed on an alumina crucible and heated continuously from 30 °C to 750 °C at a heating rate of 5 °C/min under a dynamic air atmosphere at 8 L/h. Calcinated caolinite was used as a reference material. The furnace was calibrated using transition temperature of indium. The freeze-dried Ca–PG and Ca–Al–PG networks obtained at pH 3.50 were also analysed under nitrogen atmosphere at 14 L/h. All thermal analyses were conducted in triplicate.

4.3. FT-IR spectroscopy

Infrared spectra of the freeze-dried samples (as is) diluted (1:10) with KBr (Aldrich, Chemical Co., Milwaukee, WI, USA) were recorded on a Nicolet Impact 400 FT-IR Spectrophotometer (Madison, WI). The instrument used was fitted with an apparatus for diffuse reflectance (Spectra-Tech, Inc., Stamford, CT). 200 scans at a resolution of 4 cm^{-1} were coadded and referenced against KBr.

Ca–PG and Ca–Al–PG networks obtained at pH 3.50 were heated isothermally to 400 °C (TG–DTA92, SETARAM, France) and their degradation residues were consequently analysed by FT-IR spectroscopy as for the as is samples.

Acknowledgement

This project was funded by MiUR (Ministero dell'Istruzione dell'Università e della Ricerca) PRIN 2004 (Grant number: 2004070459_003).

References

1. Thakur, B. R.; Singh, R. K.; Handa, A. K. *Crit. Rev. Food Sci.* **1997**, *37*, 47–73.
2. Grant, G. T.; Morris, R. E.; Rees, D. A.; Smith, P. J. C.; Thom, D. *FEBS Lett.* **1973**, *32*, 195–198.
3. Walkinshaw, M. D.; Arnott, S. *J. Mol. Biol.* **1981**, *153*, 1075–1085.
4. Pérez, S.; Mazeau, K.; du Penhoat Hervé, C. *Plant Physiol. Biochem.* **2000**, *38*, 37–55.
5. Thom, D.; Grant, G. T.; Morris, E. R.; Rees, D. A. *Carbohydr. Res.* **1982**, *100*, 29–42.
6. Uren, N. C. *Plant Soil* **1993**, *155/156*, 79–82.
7. Uren, N. C.; Reisenauer, H. M. *Adv. Plant Nutr.* **1988**, *3*, 79–114.
8. Hinsinger, P. *Adv. Agron.* **1998**, *64*, 225–265.
9. Uren, N. C. Types, Amount and Possible Functions of Compounds Released into the Rhizosphere by Soil-Grown Plants. In *The Rhizosphere*; Ed Pinton, R., Varanini, Z., Nannipieri, P., Eds.; Marcel Dekker: New York, Basel, 2001; pp 19–25.
10. Leppard, G. G. *Science* **1974**, *185*, 1066–1067.
11. Foster, R. C. *Rev. Phytopathol.* **1986**, *24*, 211–234.
12. Deiana, S.; Manunza, B.; Palma, A.; Premoli, A.; Gessa, C. Interactions and Mobilization of Metal Ions at the Soil–Root Interface. In *Trace Elements in the Rhizosphere*; Gobran, G. R., Wenzel, W. W., Lombi, E., Eds.; CRC Press: Boca Raton, FL, USA, 2001, pp 127–148.
13. Gessa, C.; Deiana, S. *Plant Soil* **1992**, *140*, 1–13.
14. Gessa, C.; Deiana, S. *Plant Soil* **1990**, *129*, 211–217.
15. Gessa, C.; Deiana, S.; Marceddu, S. Fibrillar Structure of Ca–Polygalacturonate as a Model for Soil–Root Interface: Metal Ion Adsorption and its Effect on the Free Space

Volume of the System In *Plant Membrane Transport: the Current Position*; Dainty, J., De Michelis, M. I., Marre, E., Rasi-Caldogno, F., Eds.; Elsevier: Amsterdam, 1989; pp 615–616.
16. Blamey, F. P. C.; Asher, C. J.; Edwards, D. C.; Kerven, G. L. *J. Plant Nutr.* **1993**, *16*, 555–562.
17. Kinraide, T. B.; Parker, D. R. *Physiol. Plant.* **1990**, *79*, 283–288.
18. Alva, A. K.; Asher, C. J.; Edwards, C. G. *Aust. J. Agric. Res.* **1986**, *37*, 375–382.
19. Gessa, C.; Deiana, S.; Premoli, A.; Ciurli, A. *Plant Soil* **1997**, *190*, 289–299.
20. Gessa, C.; De Cerchi, M. L.; Dessì, A.; Deiana, S.; Micera, G. *Inorg. Chim. Acta* **1983**, *80*, L53–L55.
21. Deiana, S.; Premoli, A.; Senette, C.; Gessa, C.; Marzadori, C. *J. Plant Nutr.* **2003**, *26*, 1927–1941.
22. Morel, J. L.; Mench, M.; Guckert, A. *Biol. Fertil. Soils* **1986**, *2*, 29–34.
23. Malovíková, A.; Rinaudo, M.; Milas, M. *Biopolymers* **1994**, *34*, 1059–1064.
24. Wellner, N.; Kačuráková, M.; Malovíková, A.; Wilson, R. H.; Belton, P. S. *Carbohydr. Res.* **1998**, *308*, 123–131.
25. Deiana, S.; Erre, L.; Micera, G.; Piu, P.; Gessa, C. *Inorg. Chim. Acta* **1980**, *46*, 249–253.
26. Synytsya, A.; Eopíková, J.; Matejka, P.; Machovič, V. *Carboydr. Polym.* **2003**, *54*, 97–106.
27. Kačuráková, M.; Wilson, R. H. *Carboydr. Polym.* **2001**, *44*, 291–303.
28. Soares, S.; Camino, G.; Levchik, S. *Polym. Degrad. Stabil.* **1998**, *62*, 25–31.
29. Soares, S.; Ricardo, N. M. P. S.; Jones, S.; Heatley, F. *Eur. Polym. J.* **2001**, *37*, 737–745.
30. Weber, J. V.; Koch, A.; Robert, D. *J. Therm. Anal.* **1998**, *53*, 11–17.
31. Waymack, B. E.; Belote, J. L.; Baliga, V. L.; Hajaligol, M. R. *Fuel* **2004**, *83*, 1505–1518.
32. Marin, N.; Krzton, A.; Koch, A.; Robert, D.; Weber, J. V. *J. Therm. Anal. Calorim.* **1999**, *55*, 765–772.
33. Mimmo, T.; Marzadori, C.; Francioso, O.; Deiana, S.; Gessa, C. *Biopolymers* **2003**, *70*, 655–661.
34. Alagna, L.; Prosperi, T.; Tomlinson, A. G.; Rizzo, R. *J. Phys. Chem.* **1986**, *90*, 6853–6857.
35. Bosco, M.; Miertus, S.; Turchini, S.; Prosperi, T.; Ascone, I.; Rizzo, R. *Carbohydr. Polym.* **2002**, *47*, 15–26.
36. Gessa, C.; Mimmo, T.; Deiana, S.; Marzadori, C. *Plant Soil* **2005**, *272*, 301–311.
37. Menzies, N. W.; Kerven, G. L.; Bell, L. C.; Edwards, D. G. *Commun. Soil Sci. Plant Anal.* **1992**, *23*, 17–20.